

RESEARCH

Open Access

Free Rhodium (II) citrate and rhodium (II) citrate magnetic carriers as potential strategies for breast cancer therapy

Marcella LB Carneiro^{1*†}, Eloiza S Nunes², Raphael CA Peixoto¹, Ricardo GS Oliveira¹, Luiza HM Lourenço¹, Izabel CR da Silva¹, Andreza R Simioni³, Antônio C Tedesco³, Aparecido R de Souza², Zulmira GM Lacava¹ and Sônia N Bão¹

Abstract

Background: Rhodium (II) citrate ($\text{Rh}_2(\text{H}_2\text{cit})_4$) has significant antitumor, cytotoxic, and cytostatic activity on Ehrlich ascite tumor. Although toxic to normal cells, its lower toxicity when compared to carboxylate analogues of rhodium (II) indicates $\text{Rh}_2(\text{H}_2\text{cit})_4$ as a promising agent for chemotherapy. Nevertheless, few studies have been performed to explore this potential. Superparamagnetic particles of iron oxide (SPIOs) represent an attractive platform as carriers in drug delivery systems (DDS) because they can present greater specificity to tumor cells than normal cells. Thus, the association between $\text{Rh}_2(\text{H}_2\text{cit})_4$ and SPIOs can represent a strategy to enhance the former's therapeutic action. In this work, we report the cytotoxicity of free rhodium (II) citrate ($\text{Rh}_2(\text{H}_2\text{cit})_4$) and rhodium (II) citrate-loaded maghemite nanoparticles or magnetoliposomes, used as drug delivery systems, on both normal and carcinoma breast cell cultures.

Results: Treatment with free $\text{Rh}_2(\text{H}_2\text{cit})_4$ induced cytotoxicity that was dependent on dose, time, and cell line. The IC_{50} values showed that this effect was more intense on breast normal cells (MCF-10A) than on breast carcinoma cells (MCF-7 and 4T1). However, the treatment with 50 μM $\text{Rh}_2(\text{H}_2\text{cit})_4$ -loaded maghemite nanoparticles (Magh- $\text{Rh}_2(\text{H}_2\text{cit})_4$) and $\text{Rh}_2(\text{H}_2\text{cit})_4$ -loaded magnetoliposomes (Lip-Magh- $\text{Rh}_2(\text{H}_2\text{cit})_4$) induced a higher cytotoxicity on MCF-7 and 4T1 than on MCF-10A ($p < 0.05$). These treatments enhanced cytotoxicity up to 4.6 times. These cytotoxic effects, induced by free $\text{Rh}_2(\text{H}_2\text{cit})_4$, were evidenced by morphological alterations such as nuclear fragmentation, membrane blebbing and phosphatidylserine exposure, reduction of actin filaments, mitochondrial condensation and an increase in number of vacuoles, suggesting that $\text{Rh}_2(\text{H}_2\text{cit})_4$ induces cell death by apoptosis.

Conclusions: The treatment with rhodium (II) citrate-loaded maghemite nanoparticles and magnetoliposomes induced more specific cytotoxicity on breast carcinoma cells than on breast normal cells, which is the opposite of the results observed with free $\text{Rh}_2(\text{H}_2\text{cit})_4$ treatment. Thus, magnetic nanoparticles represent an attractive platform as carriers in $\text{Rh}_2(\text{H}_2\text{cit})_4$ delivery systems, since they can act preferentially in tumor cells. Therefore, these nanoparticulate systems may be explored as a potential tool for chemotherapy drug development.

* Correspondence: marbretas@gmail.com

† Contributed equally

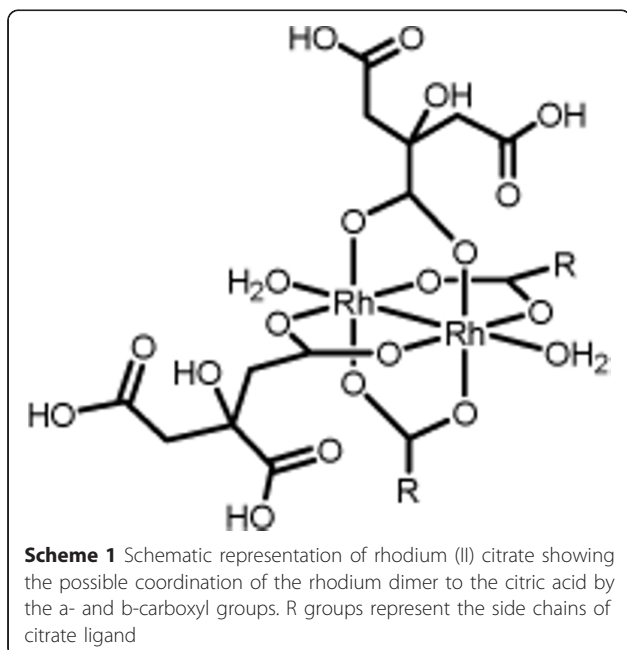
¹Instituto de Ciências Biológicas, Universidade de Brasília (UnB), Brazil. 70.919-970

Full list of author information is available at the end of the article

Background

Breast carcinoma represents the major cause of death among women worldwide. More than 410,000 deaths are estimated to occur every year, due to its high metastatic capability [1]. This fact demands a continuous development of drugs that may effectively treat breast cancer patients. In point of fact, there is a wide field of research concerning antitumor activity of metal complexes such as platinum [2], ruthenium [3], and rhodium [4]. Among these, rhodium carboxylates are known for their capacity to unpair DNA bases and therefore inhibit DNA synthesis. Their antitumor effect has already been studied on Ehrlich ascites tumor, P388 lymphocytic leukemia, oral carcinoma, L1210 and B16 melanoma, MCA mammary carcinoma and Lewis lung carcinoma [4-6].

The structure of rhodium (II) citrate ($\text{Rh}_2(\text{H}_2\text{cit})_4$), a rhodium carboxylate, is consistent with the familiar dimeric "lantern" structure with bridging carboxylates and a metal-metal bond (Scheme 1). Interestingly, $\text{Rh}_2(\text{H}_2\text{cit})_4$ has significant antitumor, cytotoxic, and cytostatic activity on Ehrlich ascites tumor [7]. Although toxic to normal cells, its lower toxicity when compared to carboxylate analogues of rhodium (II) indicates $\text{Rh}_2(\text{H}_2\text{cit})_4$ as a promising agent for chemotherapy [4]. Nevertheless, few studies have been performed to explore this potential.



$\text{Rh}_2(\text{H}_2\text{cit})_4$ presents uncoordinated functional groups (-COOH and -OH) in its structure. These groups may establish physical or chemical interactions when used in reaction steps with specific molecules or surfaces. Further, these functional groups are chemically similar

to bioactive molecules that have been used to functionalize nanostructure materials, such as magnetic nanoparticles, leading to stable colloidal suspensions with excellent biocompatibility and stability [8].

Superparamagnetic particles of iron oxide with appropriate surface functionalization/encapsulation, presented as magnetic fluids or magnetoliposomes, represent an attractive platform as carriers in drug delivery systems (DDS) because they can act specifically in tumor cells [9]. The success of magnetic nanoparticles is mainly due to their high surface area, capacity to pass through the tumor cell membrane and retention to the tumor tissue [10]. In this context, the association between $\text{Rh}_2(\text{H}_2\text{cit})_4$ and magnetic nanoparticles, in magnetic fluids or in magnetoliposomes, may work as target-specific drug delivery systems, representing a strategy for enhancement of the therapeutic action of $\text{Rh}_2(\text{H}_2\text{cit})_4$ without affecting normal cells.

Some anticancer drugs associated with magnetic nanoparticles such as doxorubicin [11], methotrexate [12], tamoxifen [13], paclitaxel [14], and cisplatin [15] have high potential for chemotherapy. Among the magnetic particles, maghemite ($\gamma\text{-Fe}_2\text{O}_3$) is suitable for clinical applications due to its magnetic properties and low toxicity [16]. In this work, we investigated the cytotoxicity induced by (1) free $\text{Rh}_2(\text{H}_2\text{cit})_4$, (2) $\text{Rh}_2(\text{H}_2\text{cit})_4$ -loaded maghemite nanoparticles (Magh- $\text{Rh}_2(\text{H}_2\text{cit})_4$) and (3) $\text{Rh}_2(\text{H}_2\text{cit})_4$ -loaded magnetoliposomes (Lip-Magh- $\text{Rh}_2(\text{H}_2\text{cit})_4$) on both normal and carcinoma breast cell cultures.

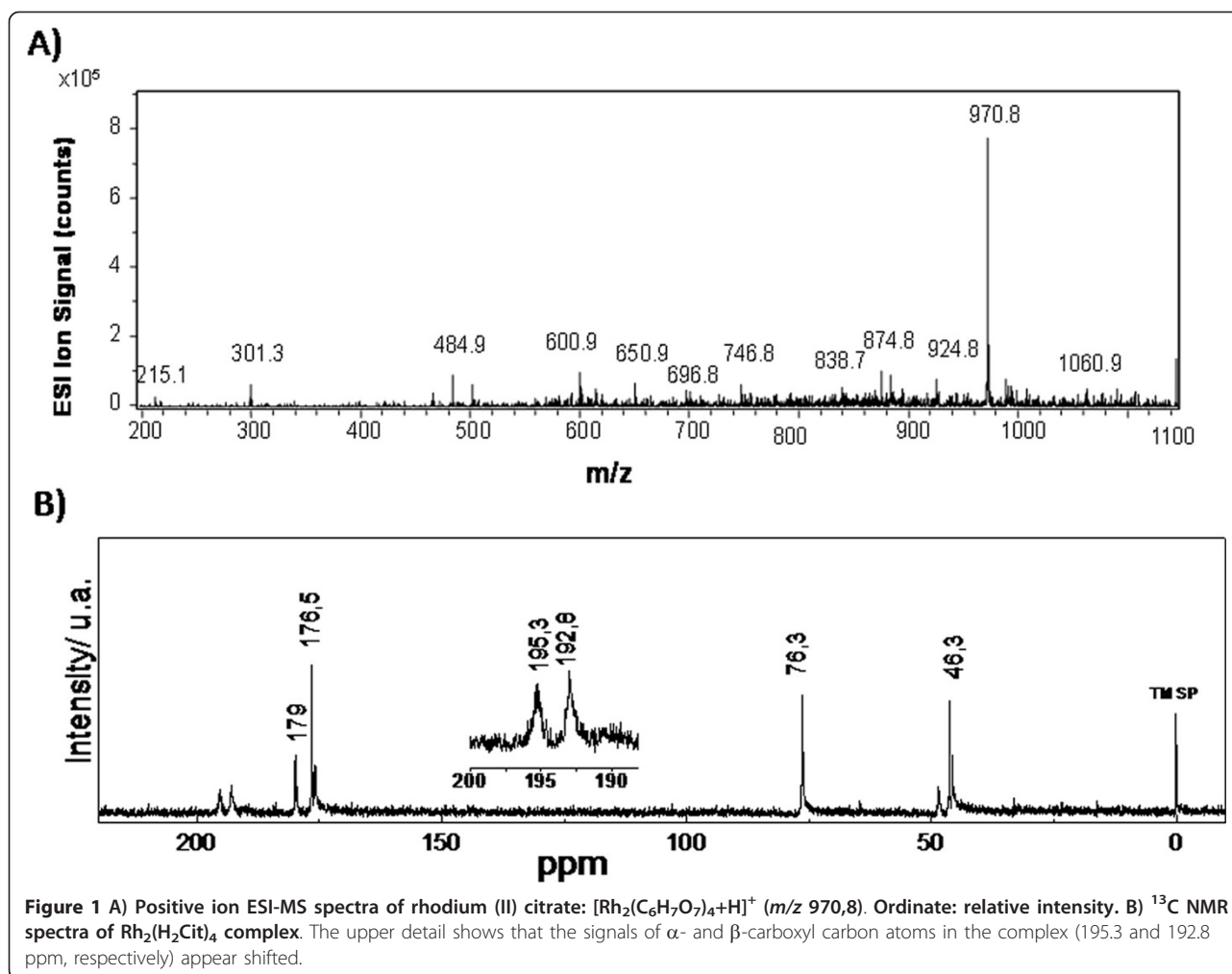
The association of $\text{Rh}_2(\text{H}_2\text{cit})_4$ to magnetic nanoparticles induced specific cytotoxic effect in carcinoma cells. Therefore, we suggest that Magh- $\text{Rh}_2(\text{H}_2\text{cit})_4$ and Lip-Magh- $\text{Rh}_2(\text{H}_2\text{cit})_4$ may be explored as potential drugs for chemotherapy.

Results

• Characterization of rhodium (II) citrate

Elemental analyses of rhodium (II) citrate sample are consistent with the molecular formula $[\text{Rh}_2(\text{C}_6\text{H}_7\text{O}_7)_4(\text{H}_2\text{O})_2]$ and suggest, in solid state, the presence of two water molecules in axial position. Thermal studies of the complex showed that the temperature ranged from 25 to 140°C, with an estimated mass loss 4.1% (calculated mass loss = 3.6%), which can be accounted for by the loss of the two water molecules. The ESI-MS spectrum of $[\text{Rh}_2(\text{C}_6\text{H}_7\text{O}_7)_4 + \text{H}]^+$ (Figure 1A) shows prominent peaks at $m/z = 970.8$, corresponding to $[\text{Rh}_2(\text{C}_6\text{H}_7\text{O}_7)_4 + 1\text{H}]^+$.

The complex was observed in a ^{13}C NMR spectrum (Figure 1B) where the signals of α - and β -carboxyl carbon atoms in the complex (195.3 and 192.8 ppm, respectively) appear shifted in comparison with those with free ligands (179 and 176.5 ppm, respectively). The shift and split of observed C-O stretching frequencies



(from 1740 to 1592 and 1412 cm^{-1}) of citric acid in infrared spectra has been used to show the coordination of citric acid to rhodium. The value of $\Delta(\nu_{\text{as}} \text{CO}_2 - \nu_{\text{s}} \text{CO}_2) = 184 \text{ cm}^{-1}$ observed in the spectrum of rhodium (II) citrate suggests the occurrence of a bridged or chelated bidentate coordination.

The titration of free carboxylic acid groups in the complex provided a ratio of $7.4 \pm 0.4 \text{ mol H}^+$ by complex mol, indicating a 8:1 stoichiometry predicted by the proposed formula $\text{Rh}_2(\text{H}_2\text{cit})_4$.

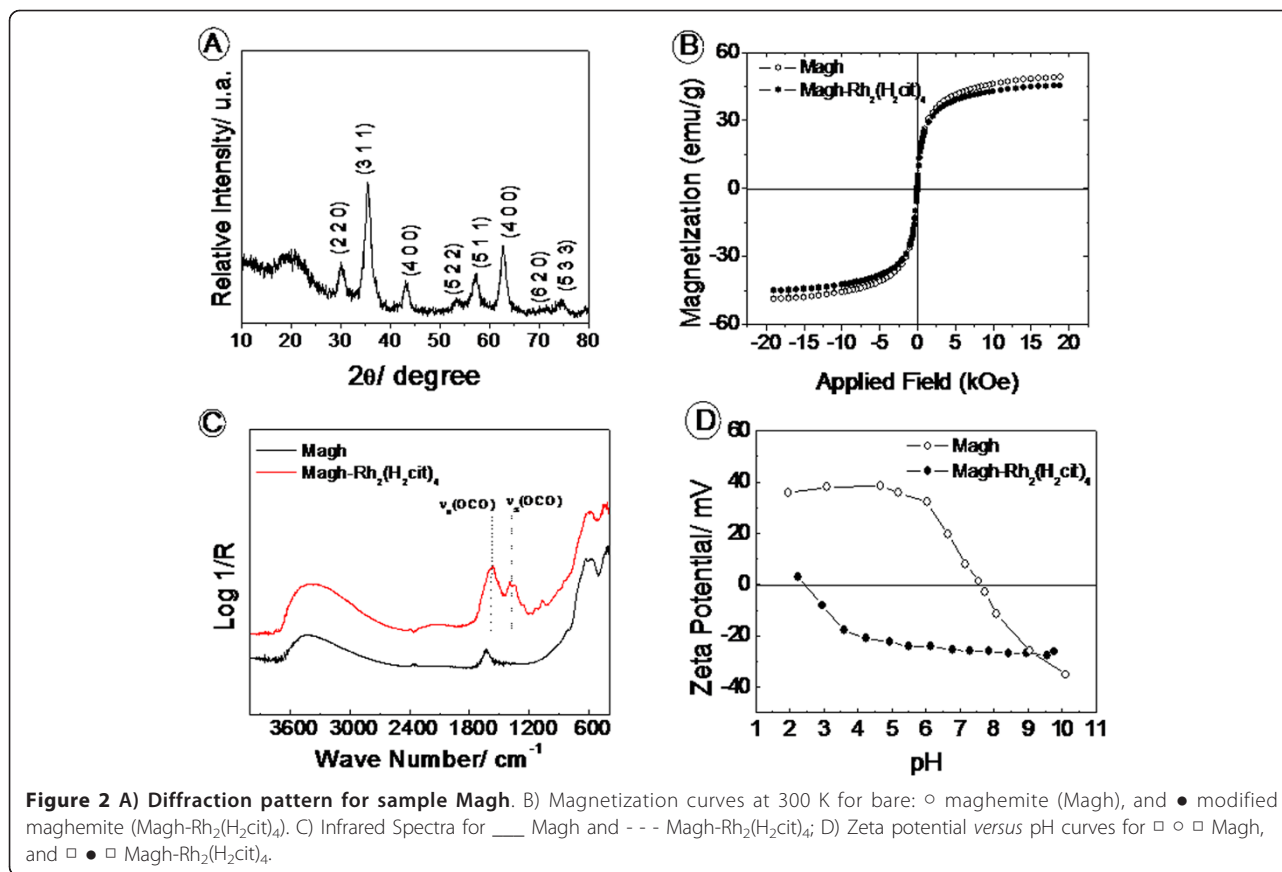
• Characterization of Magnetic Nanoparticles and Magnetoliposomes

SPIOs were obtained in the maghemite ($\gamma\text{-Fe}_2\text{O}_3$) phase and presented the characteristic diffraction patterns of inverse spinel structure when compared to reference patterns in the literature [17] for maghemite from the International Center of Diffraction Data [18] (Figure 2A). The molar ratio of $\text{Fe}^{2+}/\text{Fe}^{3+}$ obtained by elemental analysis was less than 0.015, revealing an efficient oxidation from magnetite to maghemite phase.

The magnetization curves for bare maghemite (Magh) and surface modified maghemite ($\text{Magh-Rh}_2(\text{H}_2\text{cit})_4$) are shown in Figure 2B. For both samples, the curves indicate superparamagnetic behavior, since no hysteresis was observed [19,20]. The saturation of magnetization was 48 emug^{-1} to Magh and 45 emug^{-1} to $\text{Magh-Rh}_2(\text{H}_2\text{cit})_4$.

The surface modification of maghemite nanoparticles was evidenced by infrared spectroscopy and zeta potential measurements. The infrared spectra of functionalized nanoparticles (Figure 2C) show intense absorptions in 1630 and 1564 cm^{-1} assigned to asymmetrical $\nu_{\text{as}}(\text{COO})$ and symmetrical $\nu_{\text{s}}(\text{COO})$ stretching modes of carboxylate groups [21]. These bands indicate the chemical adsorption of $\text{Rh}_2(\text{H}_2\text{cit})_4$ molecules onto the oxide surface [22]. In 1724 cm^{-1} , the stretching vibration of carboxylic acid $\nu(\text{C}=\text{O})$ is observed.

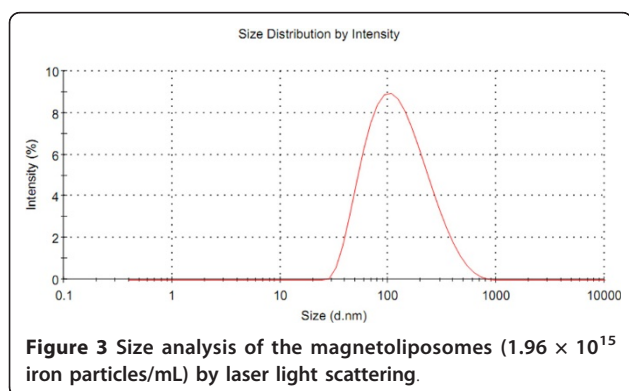
The presence of free acid groups is consistent with obtainment of stable magnetic fluids in physiological pH. The surface $\text{Magh-Rh}_2(\text{H}_2\text{cit})_4$ presented a negative zeta potential in a broad range of pH values, and its magnitude in pH 7 was about -35 mV (Figure 2D).



The complex and iron oxide content in the sample Magh-Rh₂(H₂cit)₄ were 1.4 mmolL⁻¹ and 0.33 molL⁻¹, respectively.

The magnetoliposome size presented an average measurement of 101.8 ± 0.1 nm, with polydispersion index lower than 0.22, which corresponded to 98% of the Gaussian distribution (Figure 3).

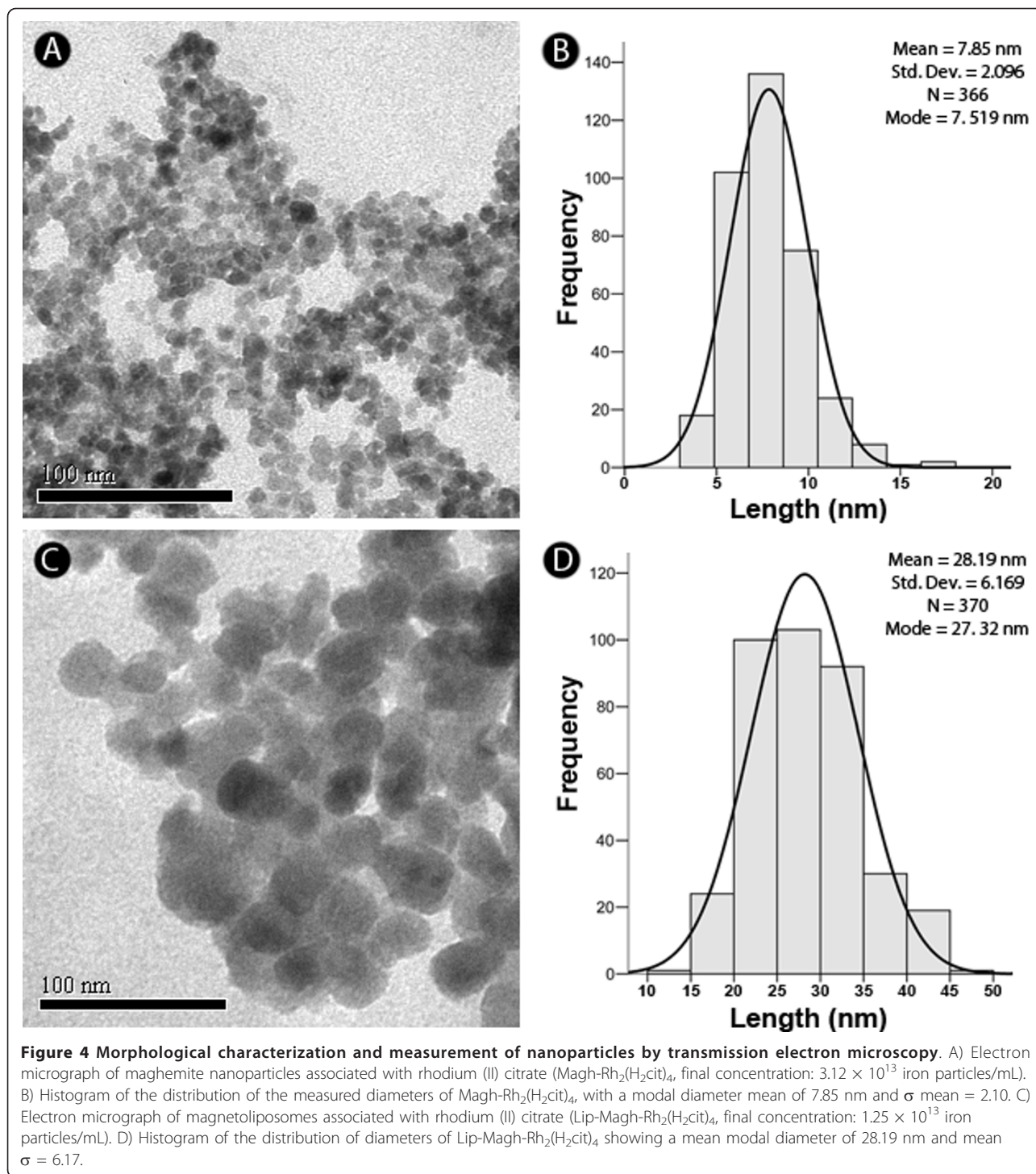
TEM micrographs revealed that the maghemite nanoparticles used (Magh-Rh₂(H₂cit)₄) have a spherical shape (Figure 4A) and a modal diameter of 7.85 nm (SD = 2.10) (Figure 4B). In contrast, samples of Lip-



Magh-Rh₂(H₂cit)₄ have a rounded shape (Figure 4C) and a modal diameter of 28.19 nm (SD = 6.17) (Figure 4D). Different sized nanoparticles were also observed in the samples, demonstrating their polydispersed distribution.

• Cytotoxicity of free rhodium (II) citrate

The distribution of cell viability according to the treatment, time, and the evaluated cell line after incubation with free rhodium (II) citrate (Rh₂(H₂cit)₄) is shown in Table 1. A significant difference in the viability of the cells with and without Rh₂(H₂cit)₄ treatment was observed, independently of the cell line and the duration of treatment ($p < 0.05$). We did not observe cytotoxicity at doses lower than 50 μ M Rh₂(H₂cit)₄ (data not shown). All cell lines presented similar cytotoxic effect of 50 μ M Rh₂(H₂cit)₄ after 24, 48, and 72 h treatments. However, at doses higher than 200 μ M, higher cytotoxicity was observed on breast normal cell line (MCF-10A) than on breast carcinoma cell lines (MCF-7 and 4T1). In general, the cytotoxic effect of Rh₂(H₂cit)₄ was higher after 72 h and after treatments with 500 and 600 μ M doses ($p < 0.05$). Thus, Rh₂(H₂cit)₄ induced a dose and time-dependent viability reduction on the investigated cell lines.



Paclitaxel (50 μM), used as positive control, induced a more intense cytotoxic effect after 72 h in the three cell lines than $\text{Rh}_2(\text{H}_2\text{cit})_4$. Treatments with DMSO caused no significant cytotoxicity to the three cell lines studied after 24 and 48 h treatments. Nevertheless, after 72 h, DMSO demonstrated a higher cytotoxicity to 4T1 and

MCF-10A cells lines than to MCF-7 line. Since the cells studied showed sensitivity to paclitaxel our experimental models were validated (Table 1).

The IC_{50} values of the treatments with $\text{Rh}_2(\text{H}_2\text{cit})_4$ in MCF-7, 4T1, and MCF-10A cells are shown in Table 2. The results confirmed that the cytotoxicity of the

Table 1 Distribution of cell viability percentage according to the treatment, cell line and exposure time

Treatment	Cell line	24 h		48 h		72 h	
0 (control)	MCF-7	100.00 ± 1.50	A*; a [#]	99.94 ± 1.95	A; a	100.00 ± 1.06	A; a
	4T1	100.00 ± 1.21	A; a	100.00 ± 1.46	A; a	100.00 ± 1.34	A; a
	MCF-10A	100.00 ± 3.30	A; a	100.00 ± 1.05	A; a	100.00 ± 0.92	A; a
Rh ₂ (H ₂ cit) ₄ 50 μM	MCF-7	94.96 ± 2.44	A; a	97.48 ± 2.84	A; a	81.19 ± 2.30	B; a
	4T1	90.31 ± 1.38	A; a	87.79 ± 2.63	A,B; a	81.42 ± 2.56	B; a
	MCF-10A	97.75 ± 3.77	A; a	97.82 ± 1.40	A; a	84.30 ± 2.55	B; a
Rh ₂ (H ₂ cit) ₄ 200 μM	MCF-7	89.28 ± 2.60	A; a	81.64 ± 2.38	A; a	70.13 ± 2.58	B; a
	4T1	79.13 ± 1.44	A; b	73.42 ± 2.17	A,B; a	68.12 ± 3.64	B; a
	MCF-10A	61.82 ± 6.54	A; b	44.19 ± 1.60	B; b	30.43 ± 2.69	C; b
Rh ₂ (H ₂ cit) ₄ 300 μM	MCF-7	85.33 ± 2.14	A; a	73.77 ± 2.58	B; a	54.14 ± 2.47	C; a
	4T1	73.95 ± 2.54	A; a	61.77 ± 1.47	B; b	47.79 ± 4.11	C; a
	MCF-10A	39.41 ± 7.47	A; b	23.81 ± 0.74	B; c	12.78 ± 0.92	C; b
Rh ₂ (H ₂ cit) ₄ 500 μM	MCF-7	50.08 ± 2.49	A; a	25.29 ± 3.46	B,C; a	30.39 ± 3.47	C; a
	4T1	46.14 ± 3.49	A; a	30.66 ± 1.22	B; a	26.07 ± 2.75	B; a
	MCF-10A	25.85 ± 6.46	A; b	11.62 ± 1.17	A,B; b	5.46 ± 0.46	C; b
Rh ₂ (H ₂ cit) ₄ 600 μM	MCF-7	28.71 ± 3.90	A; a	16.86 ± 1.77	B; a	12.16 ± 1.93	B; a
	4T1	29.87 ± 3.67	A; a	15.86 ± 0.57	B; a	9.97 ± 1.49	B; a
	MCF-10A	13.34 ± 2.43	A; b	10.26 ± 1.27	A; b	4.76 ± 0.39	B; b
DMSO (0.85%)	MCF-7	90.51 ± 5.9	A; a	90.93 ± 1.7	A; a	96.4 ± 1.4	A; a
	4T1	106.2 ± 1.3	A; b	100.6 ± 2.97	A; a	43.07 ± 8.2	B; b
	MCF-10A	148.1 ± 6.8	A; c	82.45 ± 2.3	B; a	63.35 ± 2.2	C; c
Paclitaxel 50 μM	MCF-7	70.07 ± 0.4	A; a	55.93 ± 1.6	B; a	18.92 ± 4.3	C; a
	4T1	68.31 ± 1.2	A; a	30.12 ± 0.7	B; b	21.51 ± 1.4	C; a
	MCF-10A	80.17 ± 6.7	A; c	33.52 ± 1.09	B; b	20.95 ± 1.1	C; a

The data represent the mean ± SE (mean standard error) of three independent experiments in triplicates. * Different capital letters denote statistical difference between viability in the different times (rows) for a given cell line (breast cancer cells MCF-7, 4T1 or normal cells MCF-10A) under the same treatment (p <0.05). # Different tiny letters indicate mean statistical difference between the viability of different cell lines (columns) for a given time (24, 48 or 72 hours) (p <0.05).

treatment with the complex is dependent on dose, time, and cell line. The IC₅₀ values for human carcinoma (MCF-7) and mouse carcinoma (4T1) cell lines were relatively similar. Likewise, normal cell lines (MCF-10A) were more sensitive to treatment with Rh₂(H₂cit)₄ (Table 2).

• **Analysis of morphological and structural alterations on MCF-7 and 4T1 cell lines**

MCF-7 cells have predominantly fusiform morphology (Figure 5A), while 4T1 cells presented both spindle and rounded cells forming clusters, characteristic of this these types of tumor cells (Figure 6A). Nevertheless, both MCF-7 and 4T1 cells became more rounded and

with blebbing after treatment with 500 μM Rh₂(H₂cit)₄ for 48 h. After this treatment smaller confluence and reduced cell size were also observed when 4T1 and MCF-7 control cells were compared. Furthermore, this effect was more pronounced in the 4T1 cell line (Figure 5A, B and 6A, B). No morphological alterations were observed in MCF-7 and 4T1 untreated cells (control), according to the images taken by the phase contrast microscope (Figure 5A and 6A).

Ultrastructural details of MCF-7 and 4T1 cell morphology, after treatment with 500 μM Rh₂(H₂cit)₄, are shown in Figure 5D, F and 6D, F, respectively. After this treatment, several morphological alterations were observed, such as the presence of blebbing, the

Table 2 Distribution of the IC₅₀ values and their respective confidence intervals (95%) in MCF-7, 4T1, and MCF-10A cell lines after treatment with free rhodium (II) citrate (Rh₂(H₂cit)₄)

Cell lines	IC ₅₀ (IC 95%)					
	24 hours		48 hours		72 hours	
MCF-7	483 μM	(459,2 a 507 μM)	376 μM	(356,2 a 396,1 μM)	294 μM	(259,9 a 332,5 μM)
4T1	440 μM	(407,3 a 475 μM)	337 μM	(317,3 a 357,8 μM)	271 μM	(241,4 a 303,9 μM)
MCF-10A	250 μM	(211,1 a 295,2 μM)	181 μM	(172,3 a 190,8 μM)	123 μM	(114,7 a 132,7 μM)

These data refers from viability of cells after treatment with Rh₂(H₂cit)₄ (50-600 μM) for 24, 48 and 72 hours.

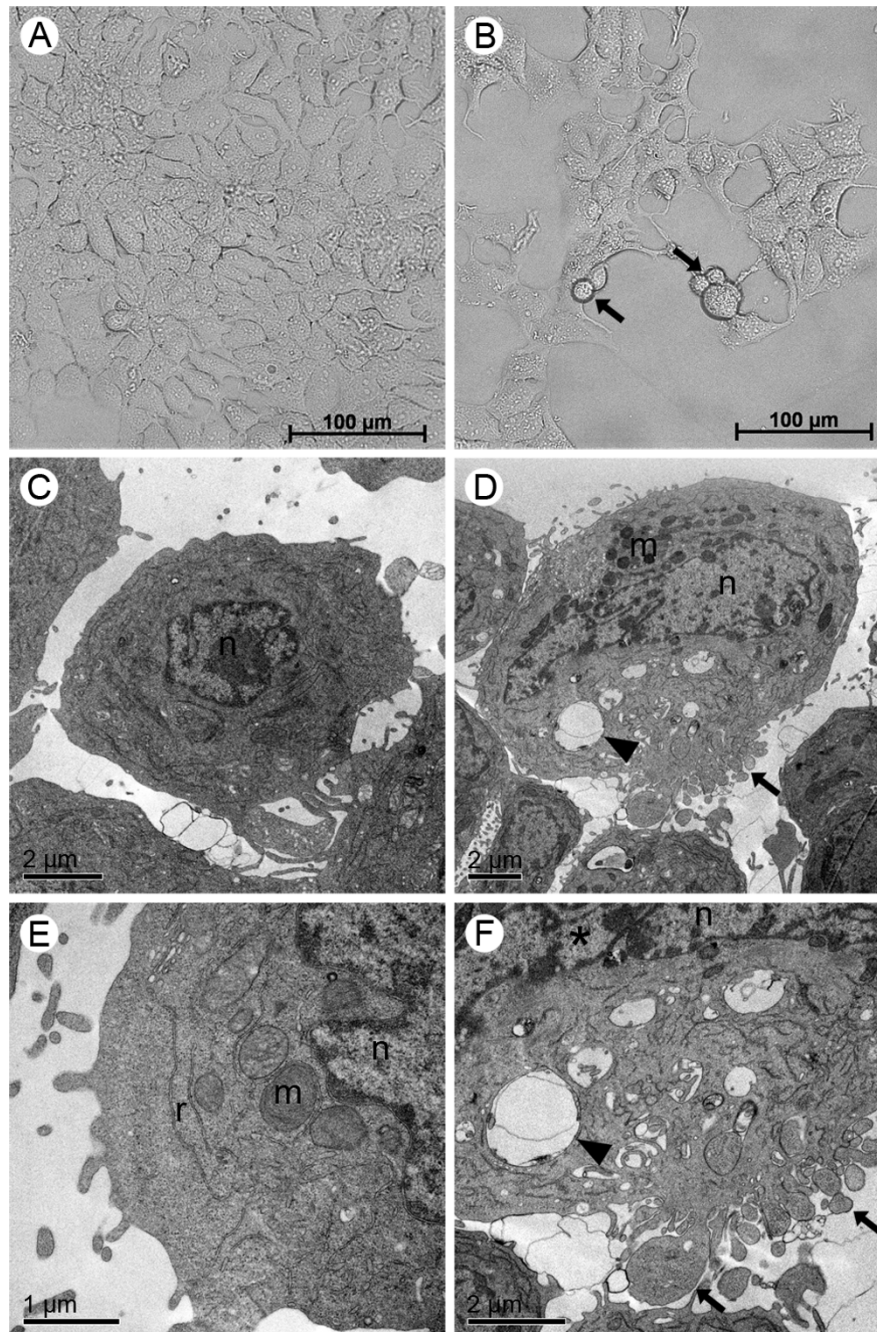


Figure 5 Morphological and structural changes induced by rhodium (II) citrate ($\text{Rh}_2(\text{H}_2\text{cit})_4$) in MCF-7 breast carcinoma cell line after 48 hours of treatment. Cells were incubated with 500 μM $\text{Rh}_2(\text{H}_2\text{cit})_4$ for 48 hours and examined by phase contrast microscopy (A, B) and transmission electron microscopy (C-F). (A, C and E) control (cells without treatment); (B, D and F) cells treated with 500 μM of $\text{Rh}_2(\text{H}_2\text{cit})_4$. Differences were observed in cell morphology, vacuole amount and mitochondrial condensation between untreated cells (A, C and E) and $\text{Rh}_2(\text{H}_2\text{cit})_4$ treated cells (B, D and F). Legends: blebbing (arrows), vacuoles (arrow heads), nucleus (n), mitochondria (m), condensed chromatin (*).

segregation of condensed chromatin to nuclear periphery and the remarkable presence of vacuoles and condensed mitochondria when compared to the MCF-7 and 4T1 control cells (Figure 5C-F and 6C-F), respectively. These morphological changes can be related to the apoptotic events.

• Phosphatidylserine exposition on breast carcinoma cells
In Figure 7 the percentage of cells that were positively stained for annexin V-FITC is represented. After 500 μM $\text{Rh}_2(\text{H}_2\text{cit})_4$ treatment, the annexin-V⁺ cell number (%) was significantly higher than that of the control in both cell lines ($p < 0.05$). After this treatment,

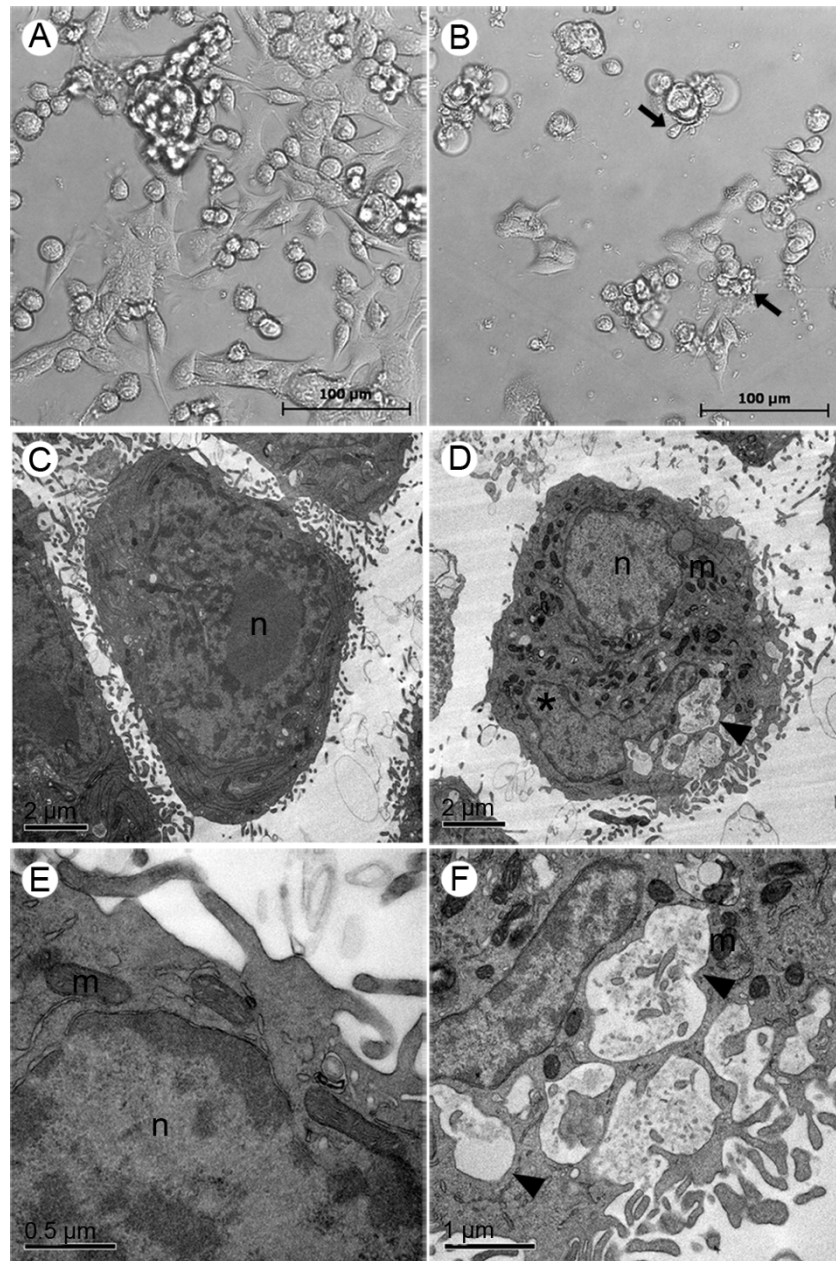
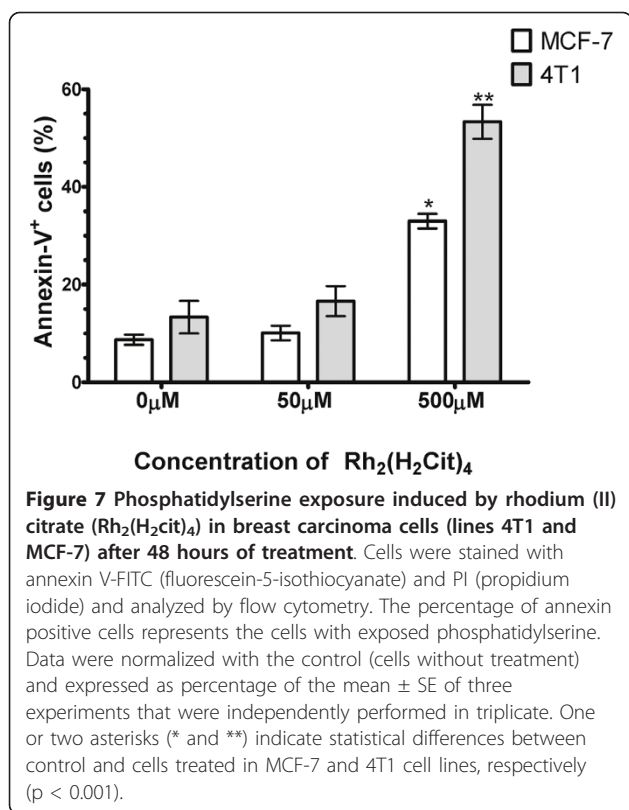


Figure 6 Morphological and structural changes induced by rhodium (II) citrate ($Rh_2(H_2cit)_4$) in 4T1 breast carcinoma cell line after 48 hours of treatment. Cells were incubated with 500 μM $Rh_2(H_2cit)_4$ for 48 hours and examined by phase contrast microscopy (A, B) and transmission electron microscopy (C-F). (A, C and E) control (cells without treatment); (B, D and F) cells treated with 500 μM of $Rh_2(H_2cit)_4$. Differences were observed in cell morphology, vacuole amount and mitochondrial condensation between untreated cells (A, C and E) and $Rh_2(H_2cit)_4$ treated cells (B, D and F). Legends: blebbing (arrows), vacuoles (arrow heads), nucleus (n), mitochondria (m), condensed chromatin (*).

there was a 25% and a 38% increase of annexin- V^+ cell number in MCF-7 and 4T1, respectively ($p < 0.05$), thus revealing that the 4T1 cell line was more sensitive to treatment with $Rh_2(H_2cit)_4$ (500 μM). No difference in the percentage of annexin- V^+ cell number was observed in relation to untreated cells (control) and 50 μM $Rh_2(H_2cit)_4$ treated cells, in both cell lines ($p < 0.05$).

• Analysis of nuclear fragmentation and actin alterations
MCF-7 cells without treatment (control) showed organized spread actin in the cytoplasm and interactions between surrounding cells through membrane projections supported by actin (Figure 8A). After treatment with 50 μM $Rh_2(H_2cit)_4$, slight nuclear condensation and reduction of actin filaments were observed



(Figure 8C). Nevertheless, a noticeable reduction in actin and increased nuclear condensation were observed after treatment with 500 μM (Figure 8E). In general, the cells treated with Rh₂(H₂cit)₄ showed a loss of cytoplasmic projections when compared to the control cells (Figure 8A, C and 8E). Furthermore, the cells treated with paclitaxel (50 μM) showed nuclear condensation and fragmentation and a lower amount of actin cytoskeleton, similar to those treated with Rh₂(H₂cit)₄ (Figure 8G). Phase contrast images were shown to validate DAPI and phalloidin-Alexa Fluor 488 staining for each experimental group (Figure 8B, D, F and 8H).

• **Cytotoxicity of rhodium (II) citrate-loaded magnetic nanoparticles**

MCF-7, 4T1, and MCF-10A cell viabilities were similar after treatment with 50 μM of free Rh₂(H₂cit)₄, independent of the treatment duration (Figure 9). Nevertheless, treatment with 50 μM Rh₂(H₂cit)₄-loaded maghemite nanoparticles (Magh-Rh₂(H₂cit)₄) and Rh₂(H₂cit)₄-loaded magnetoliposomes (Lip-Magh-Rh₂(H₂cit)₄) induced a significant decrease, mainly in MCF-7 and 4T1 breast carcinoma cell viability (p < 0.05). This effect was more evident in 4T1 cells, which showed a fall in viability of 46% (± 2.7), 69% (± 2), and 74% (± 1.4) after Magh-Rh₂(H₂cit)₄ treatment for 24, 48, and 72 h,

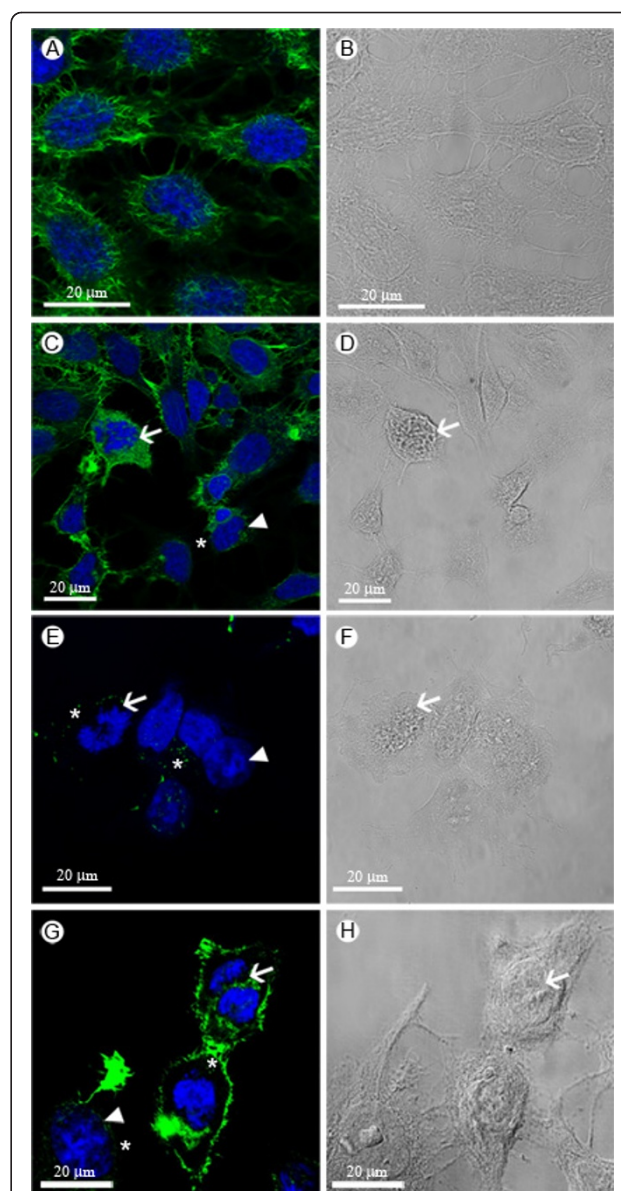
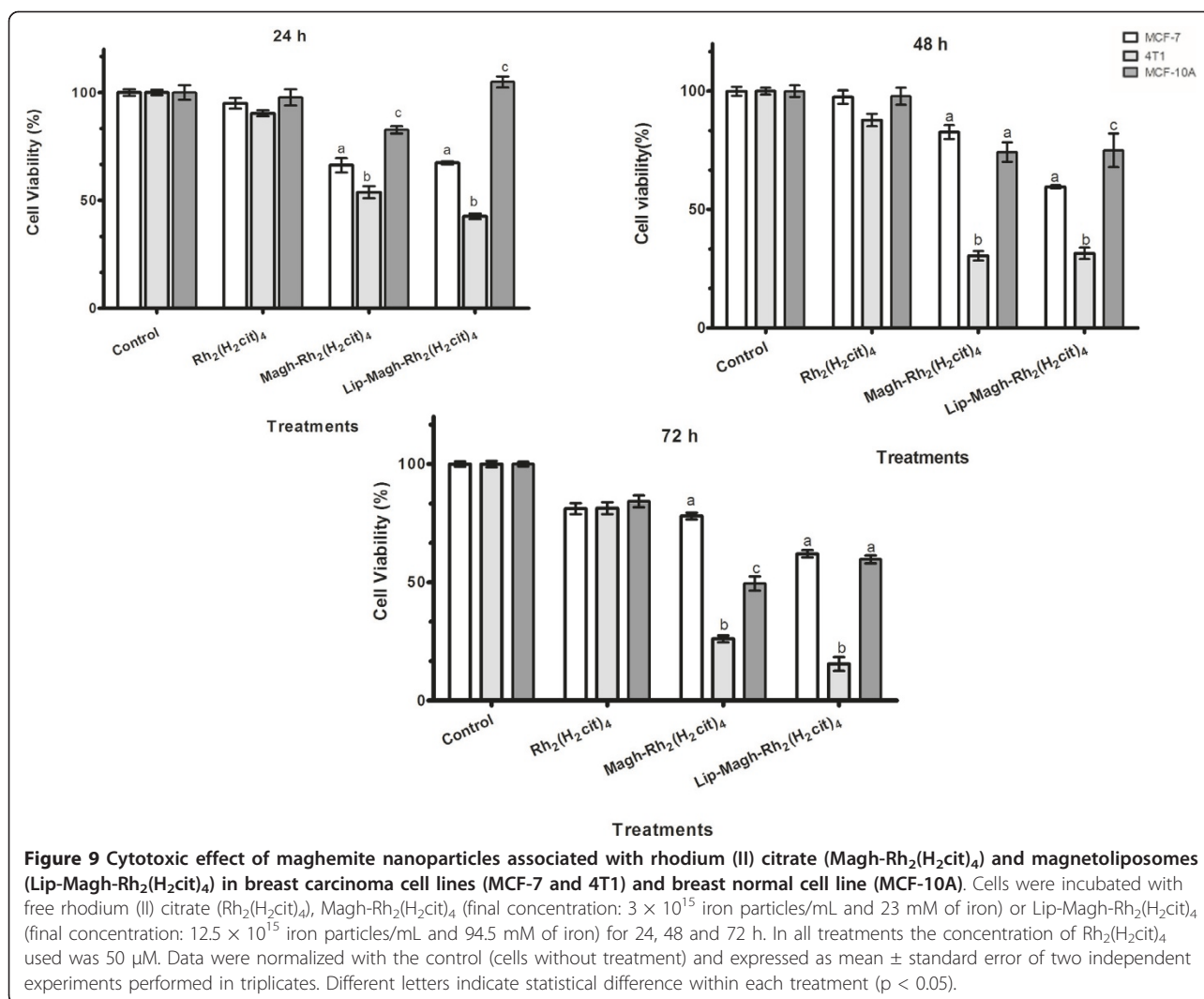


Figure 8 Nuclear fragmentation and reduction of actin filaments in MCF-7 breast carcinoma cells 48 hours after treatment. Cells were stained with DAPI (4',6-diamidino-2-fenilindol) to visualize the nucleus (in blue) and with Phalloidine-Alexa Fluor 488 to visualize actin (in green). (A, B) control (cells without treatment); (C, D) cells treated with 50 μM and (E, F) with 500 μM of Rh₂(H₂cit)₄; (G, H) cells treated with 10 nM paclitaxel for 2 h. Arrows and arrow heads indicate nuclear fragmentation and chromatin condensation, respectively. Phase-contrast images are presented for validation of fluorescence (Figure 8B, D, F, H).

respectively. Within the same time frame, the Lip-Magh-Rh₂(H₂cit)₄ treatment decreased 4T1 cell viability by 57% (± 1.3), 68% (± 2.4), and 84% (± 2.9) after 24, 48 and 72 h treatments, respectively (Figure 9). In contrast, the same dose of free Rh₂(H₂cit)₄ reduced cell viability by about 10% (± 1.4), 12% (± 2.6), and 18% (± 2.6), after



24, 48 and 72 h treatments, respectively ($p < 0.05$). However, 72 h of Magh-Rh₂(H₂cit)₄ and Lip-Magh-Rh₂(H₂cit)₄ treatments on 4T1 cells induced a decrease in cell viability of respectively 74% (± 1.4) and 84% (± 2.9) against 18% (± 2.6) presented by the free drug at the same concentration. Thus, Magh-Rh₂(H₂cit)₄ and Lip-Magh-Rh₂(H₂cit)₄ treatments showed enhanced Rh₂(H₂cit)₄ potency of up to 3.9 and 4.6 times, respectively.

Longer treatments enhanced the cytotoxicity of both Magh-Rh₂(H₂cit)₄ and Lip-Magh-Rh₂(H₂cit)₄ (Figure 9). After 24 h of treatment with Magh-Rh₂(H₂cit)₄ and Lip-Magh-Rh₂(H₂cit)₄, a differential cytotoxicity was observed among the three cell lines. This effect was more pronounced in 4T1 and MCF-7 cells. Further, we observed that Lip-Magh-Rh₂(H₂cit)₄ treatment was more cytotoxic than Magh-Rh₂(H₂cit)₄ to MCF-7 cell line ($p < 0.05$). A higher cytotoxicity was noticed in MCF-10A 72 h after the Magh-Rh₂(H₂cit)₄ treatment, but this did not happen with the Lip-Magh-Rh₂(H₂cit)₄ treatment. It is noteworthy

that in all time windows and all tested cell lines there was no difference in the viability of the control cells ($p < 0.05$) (Figure 9).

The cells treated with maghemite nanoparticles without rhodium (II) citrate (Magh) showed no reduction in viability after any treatment duration; however, viability reduction was observed after 72 h treatment with Lip-Magh (data not shown).

Discussion

In this work, the rhodium (II) citrate was isolated from the aqueous solution as powder and not as a single crystal. Due to this fact the complete structure determination cannot be resolved. However, the elemental analysis, ¹³C NMR, IR, UV/Visible data enable us to predict that the compound structure was similar to the previously studied rhodium (II) carboxylates [23]. In the ¹³C NMR spectrum (Figure 1B), the signals of α - and β -carboxyl carbon atoms in the complex appear shifted in comparison with

those for the free ligand, showing that the citrate anion is coordinated through these two carboxyl groups. In the carbinol carbon atoms, however, only a small shift is observed, indicating that there is no participation of this group in coordination [24,25]. Evidence of the coordination of citric acid ligand to rhodium through its carboxyl group was also obtained by infrared spectra, and it was similar to that reported by Najjar and co-workers for rhodium (II) citrate [26]. The coordination by the two different carboxyl groups suggests the formation of five isomeric structures; however, for the development of this work these hypothetical isomers were not separated.

The crystalline structure of magnetic nanoparticles could be confirmed by X-ray diffractometry as maghemite phase. According to Magh and Magh-Rh₂(H₂cit)₄ magnetization curves profile (Figure 2B), the nanoparticles present superparamagnetic behavior at room temperature and saturation magnetization close to values already published in the literature for 7 nm maghemite. The effect of the complex on the particle's surface to saturation magnetization is negligible [27].

Surface functionalization of SPIO with rhodium (II) citrate produced deep changes in the nanoparticles' physical-chemical properties. These changes were evidenced by infrared spectroscopy and zeta potential measurements, as well as by saturation of magnetization. The infrared spectra of Magh-Rh₂(H₂cit)₄ (Figure 2C) showed intense absorptions assigned to asymmetrical ν_{as} (COO) and symmetrical ν_s (COO) stretching modes of carboxylate groups [21], indicating the chemical adsorption of Rh₂(H₂cit)₄ molecules into the oxide surface [22]. Zeta potential *versus* pH measurements indicated an isoelectric point (iep) at about pH 3. The zeta potential becomes negative in the range of pH above 3 and its magnitude at pH 7 is about -38 mV. This zeta potential value shows that the particles are negatively charged and indicates an efficient electrostatic stabilization.

It is well known that the magnetic properties of nanomaterials are dependent on their size. Particles smaller than 10 nm, besides having high magnetic applicability, are also ideal to avoid recognition by the mononuclear phagocyte system and, thus, stay longer in the bloodstream [16]. Considering the particle size, Magh-Rh₂(h₂cit)₄ has potential for applications in the biological system as it presents a modal diameter of 7.5 nm. Moreover, considering the magnetoliposome size, as determined by zetasizer equipment (Figure 3), we could conclude that the small lipid bilayer vesicle will increase the interaction of the active compounds with cells as a normal behavior of other liposomal drug delivery systems (DDS) of similar size carrying similar nanoparticles to the cellular target [28].

In our *in vitro* study, we observed that cell lines MCF-7, 4T1, and MCF-10A exhibited cytotoxicity when treated with Rh₂(H₂cit)₄. It is reported that others

carboxylates such as acetate, butyrate, and propionate of rhodium, in association with isonicotinic acid, also induces cytotoxicity in tumor cells (K562 leukemia cell line) [29]. We also observed that Rh₂(H₂cit)₄ cytotoxicity was dose and time dependent. High concentrations of Rh₂(H₂cit)₄ (up to 200 μ M) were seen to induce greater cytotoxicity after longer treatments (72 hours). Furthermore, it was also demonstrated that its cytotoxic effect differed between breast normal (MCF-10A) and breast carcinoma (4T1 and MCF-7) cell lines, being more pronounced in breast normal cells (Table 1 and 2). Our data are, therefore, in agreement with a number of other preliminary studies. For instance, preliminary studies showed that rhodium (II) citrate induces a higher cytotoxicity, with increasing dose and duration of treatment, on breast carcinoma cells (Ehrlich) and on carcinoma (Y-1) and normal adrenocortical cells (AR-1(6)) [7]. Similarly, it was also reported that other rhodium carboxylates such as acetate, methoxyacetate, propionate, and butyrate inhibited the proliferation of leukemia cells (L1210), inducing cytotoxic effects in a dose and a time-dependent manner [30].

Several studies reported promising antitumor activities of rhodium carboxylates in mouse bearing Ehrlich breast carcinoma, but their clinical use has been limited because they showed toxicity in normal cells [4,31]. In our study, Rh₂(H₂cit)₄ was also cytotoxic to *in vitro* normal cells. The IC₅₀ values (Table 2) showed that Rh₂(H₂cit)₄ cytotoxic effect was more intense on breast normal cells (MCF-10A) than on breast carcinoma cells (MCF-7 and 4T1). However, according to the IC₅₀ values (Table 2), we demonstrated that rhodium (II) citrate is less toxic to normal cells than are members of the lipophilic complex, such as propionate, butyrate, and acetate of rhodium [30]. Therefore, this complex may have a higher chemotherapeutic potential in relation to other carboxylates. The distinctness of cytotoxicity among lipophilicity or hydrophilicity carboxylates could be explained by the differences among their properties, such as chain length and hydrophilicity of parts of the molecules [4].

The cytotoxic activity of some rhodium carboxylates is given by their ability to bind covalently to DNA bases, unpairing them, and subsequently inhibiting DNA replication and transcription [5,7]. It was reported that rhodium carboxylates establish adducts through their axial ligands with electron donor atoms, preferably N, S, O, and P, from molecules such as adenine, cysteine, and RNase A [32]. Moreover, enzymes with free thiol groups (-SH) are known to interact irreversibly with these metal complexes [30]. This interaction could explain the inactivation of some essential DNA replication enzymes which result in their damage. Thus, Rh₂(H₂cit)₄ is toxic to both normal and carcinoma cells since they need

DNA replication and transcription to survive. Zyngier and colleagues [7] demonstrated that $\text{Rh}_2(\text{H}_2\text{cit})_4$ inhibited DNA synthesis of breast carcinoma (Ehrlich), and also of carcinoma (Y-1) and, normal adrenocortical cells (AR-1(6)). We observed fragmentation nucleus induced by $\text{Rh}_2(\text{H}_2\text{cit})_4$ (Figure 5D and 6D, Figure 8C and 8E). These observations suggest that $\text{Rh}_2(\text{H}_2\text{cit})_4$ not only induces DNA fragmentation on MCF-7 and 4T1 cells, but may also prevent their DNA synthesis.

According to our TEM observations, the MCF-7 and 4T1 cells exhibited condensed mitochondria after $\text{Rh}_2(\text{H}_2\text{cit})_4$ treatment (Figure 5D, F and 5F), indicating that this organelle is somehow affected by the complex. This condensed mitochondria phenotype can be associated with a drop in the mitochondrial membrane potential related to the cell death process [33].

We observed that $\text{Rh}_2(\text{H}_2\text{cit})_4$ induced an increase in the number of vacuoles compared to the untreated cells, as shown in TEM (Figure 5 and 6). It can indicate a degradation pathway related to the response to metabolic stress or microenvironmental conditions to ensure energy balance. Moreover, this increase has been implicated in the cell death process [34,35].

After 48 h of treatment with 500 μM $\text{Rh}_2(\text{H}_2\text{cit})_4$, an increase of annexin- V^+ breast carcinoma cells was observed (Figure 7). The presence of annexin- V^+ in cells is related to apoptotic events, since it indicates the exposure of phosphatidylserine outside the inner membrane. The actin analysis performed by confocal microscopy showed a dose-dependent disassembly of the actin cytoskeleton after $\text{Rh}_2(\text{H}_2\text{cit})_4$ treatment in the MCF-7 cell (Figure 8). Furthermore, there was a notable reduction in intercellular communication, possibly caused by changes in the actin cytoskeleton (Figure 8). This structure is an important target for many antitumor drugs since it plays a crucial role in maintaining cell morphology, mitosis, signaling regulation for cell survival, and cell motility [36-38]. We demonstrated that the reduction of actin after $\text{Rh}_2(\text{H}_2\text{cit})_4$ treatment (500 μM) is intrinsically related to the higher cytotoxicity of this complex in MCF-7 cells (Table 1 and Figure 8).

In summary, $\text{Rh}_2(\text{H}_2\text{cit})_4$ induces alterations in the treated cells that are related to the apoptosis process, such as nuclear fragmentation, blebbing, disassembly of the actin cytoskeleton, and phosphatidylserine exposure in the plasma membrane. These features suggest that $\text{Rh}_2(\text{H}_2\text{cit})_4$ has potential as an efficient chemotherapeutic agent since targeting of chemotherapeutic agents is related to its capacity to induce apoptosis.

In order to reduce the toxicity of $\text{Rh}_2(\text{H}_2\text{cit})_4$ for normal cells while enhancing the efficacy in carcinoma therapy, we proposed its association with magnetic nanoparticles. Doses of 50 μM of $\text{Rh}_2(\text{H}_2\text{cit})_4$ -loaded to maghemite nanoparticles and to magnetoliposomes were

more cytotoxic than the equimolar dose of free $\text{Rh}_2(\text{H}_2\text{cit})_4$. Besides, the treatment with 50 μM of Magh- $\text{Rh}_2(\text{H}_2\text{cit})_4$ induced cytotoxicity similar to a tenfold dose of the free complex on carcinoma cells. In addition, the Magh- $\text{Rh}_2(\text{H}_2\text{cit})_4$ and Lip-Magh- $\text{Rh}_2(\text{H}_2\text{cit})_4$ induced time-dependent cytotoxic effect like those of free $\text{Rh}_2(\text{H}_2\text{cit})_4$. After 72 h, for example, Magh- $\text{Rh}_2(\text{H}_2\text{cit})_4$ and Lip-Magh- $\text{Rh}_2(\text{H}_2\text{cit})_4$ treatments enhanced cytotoxicity potency up to 3.9 and 4.6 times, respectively. More importantly, MCF-7 and 4T1 carcinoma breast cells were more susceptible to Magh- $\text{Rh}_2(\text{H}_2\text{cit})_4$ and Lip-Magh- $\text{Rh}_2(\text{H}_2\text{cit})_4$ treatments than MCF-10A normal breast cells, differently from what is observed with free $\text{Rh}_2(\text{H}_2\text{cit})_4$ (Table 2 and Figure 9).

Carcinoma and normal cells present different metabolism in relation to iron uptake. The metabolism of breast carcinoma cells, for example, is faster than in normal cells. Consequently, carcinoma cells require larger amounts of micronutrients, particularly iron, which can be evidenced by the presence of more transferrin receptors in these [39]. In this way, an increased iron uptake by tumor cells could result in a selective uptake and a higher retention of Magh- $\text{Rh}_2(\text{H}_2\text{cit})_4$ and Lip-Magh- $\text{Rh}_2(\text{H}_2\text{cit})_4$ in relation to free $\text{Rh}_2(\text{H}_2\text{cit})_4$ complex. Additionally, magnetic nanoparticle uptake by carcinoma cells may also be associated with the amino group's coverage of nanoparticles [40]. The literature reports that free thiol groups (-SH) interact with the rhodium carboxylates, which are rich in carboxylic groups [30]. Therefore, the carboxylic groups present in Magh- $\text{Rh}_2(\text{H}_2\text{cit})_4$ citrate molecules could improve the transport of nanoparticles through the cell membrane via the proteic thiol groups.

Although rhodium (II) citrate-coated maghemite nanoparticles seem not to have been described before, the association of rhodium complex with polymeric microspheres of hydroxy-propyl-cyclodextrin [41] and with cyclodextrins from hydroxyapatite has been reported [42]. These associations were shown to represent a promising alternative in the minimization of the nonspecific toxicity of these agents, mainly because they increase the efficiency of encapsulation and the duration of rhodium (II) citrate release. Our study demonstrated that the composition of maghemite nanoparticles coated with citrate or rhodium (II) citrate was appropriate for its application as a drug delivery system. Coating with the citrate molecule was able to stabilize our magnetic nanoparticles and also was not toxic to the investigated cells (data not shown). Citrate-functionalized-maghemite has been attested as providing successful nanoparticles in the production of biocompatible and stable magnetic fluids [43,44]. Furthermore, citrate-functionalized-maghemite was also shown to be internalized by *in vitro* human melanoma cells (SKMEL 37) with no significant cytotoxicity even when cultivated for 72 h [45].

We demonstrated that Magh-Rh₂(H₂cit)₄ and Lip-Magh-Rh₂(H₂cit)₄ compositions reduced more efficiently the viability of MCF-7 and 4T1 breast carcinoma cells than the free Rh₂(H₂cit)₄ treatment. Furthermore, it is important to emphasize that the cytotoxicity induced by both Magh-Rh₂(H₂cit)₄ and Lip-Magh-Rh₂(H₂cit)₄ was greater in tumor cells than normal ones, since no cytotoxicity was observed after treatment with Magh. In addition, if these nanosystems were associated to target molecules for breast carcinoma cells such as folic acid, for instance, their potential for selective uptake would be even higher [46]. Thus, Magh-Rh₂(H₂cit)₄ and Lip-Magh-Rh₂(H₂cit)₄ have much potential for application in drug delivery systems, and they should be considered as a platform to enhance Rh₂(H₂cit)₄ cytotoxicity, specifically in breast carcinoma.

Conclusions

We showed that Rh₂(H₂cit)₄ induces significant cytotoxic effects, especially after longer treatments and at higher concentrations. These effects were related to several structural and morphological alterations, probably coming from cell death by apoptosis and autophagy. Further, higher cytotoxicity in the MCF-10A breast normal cell line was noted than in the 4T1 and MCF-7 breast cancer cell lines. Nonetheless, the Magh-Rh₂(H₂cit)₄ and Lip-Magh-Rh₂(H₂cit)₄ treatments were more selective to breast cancer cells with up to 4.6 times enhanced potency in comparison to the free Rh₂(H₂cit)₄. Therefore, we suggest that Magh-Rh₂(H₂cit)₄ and Lip-Magh-Rh₂(H₂cit)₄ should be considered a suitable and effective platform for drug delivery systems that operate more specifically in tumor cells.

Methods

Materials

All solvents and reagents related to the synthesis of Rh₂(H₂cit)₄ and Magh-Rh₂(H₂cit)₄ are of analytical grade and were used without further purification: iron(II) chloride tetrahydrate (Acros); iron (III) chloride hexahydrate (Ecibra); hydrated rhodium (III) chloride (Sigma-Aldrich); citric acid (Vetec), and sodium hydroxide (FMaia). The rhodium(II) trifluoroacetate, [Rh₂(tfa)₄], was prepared following a previously reported procedure [47].

• Characterization of Rhodium Compounds

Infrared spectra were recorded using KBr pellets on a Bomem BM100 FT-IR spectrometer in the 4000-500 cm⁻¹ region. Elemental analyses were carried out on a Perkin-Elmer 2400 analyzer. Rhodium concentrations were measured in Spectro Ciros CCD ICP-AES spectrometer. The samples were digested with concentrated HCl in an aqueous solution. Electronic spectra were recorded in the

800-200 nm range on Beckman DU70 spectrometer in water solution. The ¹³C NMR spectra (carbon-13 nuclear magnetic resonance spectroscopy) were obtained at room temperature in D₂O using a Bruker Avance III 500 spectrometer, operating at a frequency of 125.75 MHz. The ¹³C chemical shifts were measured relative to TMS (tetramethylsilane) measurements. TGA (thermogravimetric analysis) was performed at a heating rate of 10°C min⁻¹ in the temperature range of 25-1000°C, under nitrogen flow of 10 mL min⁻¹ using a Shimadzu DTG-60 instrument and standard aluminum crucible. The ESI mass spectra (Electrospray ionisation-mass spectrometry) were acquired using a Bruker Daltonics Esquire 3000 Plus mass spectrometer in capillary exit voltage set at 4 kV and the desolvation chamber temperature was set to 280°C. Potentiometric titration of an aqueous solution of Rh₂(H₂cit)₄ 0.0051 molL⁻¹ was performed in triplicate using a 0.046 molL⁻¹ NaOH solution as titrant.

• Characterization of Magnetic Nanoparticles

X-ray powder diffraction (XRD) data were collected by a XRD-6000 diffractometer. The magnetization of the iron oxide nanoparticles was measured at room temperature using a vibrating-sample magnetometer (EV9-VSM AdMagnets). The iron concentration in the fluids was determined by the method of *o*-phenanthroline [48]. Solution absorbances were measured at 512 nm in a Hitachi U1100. Zeta potential was obtained from electrophoretic mobility (em) measurements performed by phase analysis light scattering using ZetaSizer Nano ZS ZEN3600 (Malvern, UK) equipment. The mean hydrodynamic particle size of Magh-Rh₂(H₂cit)₄ was determined in water by dynamic laser light scattering (DLS) and the correlation functions were evaluated by cumulant analysis. Maghemite nanoparticles were dispersed in an electrolyte (0.005 molL⁻¹ NaCl) solution to get a 0.05 molL⁻¹ iron content.

Moreover, to determine the nanoparticles' shape and size by transmission electron microscopy (TEM) an aliquot (10 µL) of synthesized (Magh-Rh₂(H₂cit)₄) (0.2%) and Lip-Magh-Rh₂(H₂cit)₄ (0.4%) was deposited on a copper grid (300 mesh), previously covered with Formvar (0.7%), and dried at room temperature. It was then observed under transmission electron microscopy (TEM, JEOL 1011, 100kV) and the images were captured by a Gatan Ultrascan camera. Nanoparticles (n = 370) were measured by Image Pro-Plus 5.1 software and data were adjusted by log normal distribution to obtain the modal diameter.

• Synthesis of the Rhodium (II) Citrate Complex, Rh₂(H₂cit)₄

Firstly, an aqueous solution of rhodium (II) trifluoroacetate (*c.a.* 1 mmol) was slowly added to a solution of citric acid (*c.a.* 10 mmol) in water under stirring and heated to

70°C. The solvent was reduced almost to dryness followed by addition of water, and this process was repeated four times. The product was dissolved in methanol and precipitated with petroleum ether and acetone 50:50 (v/v). The solid was washed with ethyl acetate about twenty times to eliminate the excess of ligand.

Yield: 20%. Anal. Calc for $[\text{Rh}_2(\text{C}_6\text{H}_8\text{O}_7)_4(\text{H}_2\text{O})_2]$: C, 28.64; H 3.2; Rh, 20.4; H_2O , 3.5%. Found: C, 28.5; H, 3.6; Rh, 20.8; H_2O , 4.41%. IR (KBr): $\nu(\text{COOH})$ 1724s; $\nu_{\text{as}}(\text{CO}_2)$ 1598vs; $\nu_{\text{s}}(\text{CO}_2)$ 1411vs cm^{-1} . ESI-MS (m/z) for $[\text{Rh}_2(\text{C}_6\text{H}_7\text{O}_7)_4+\text{H}]^+$: 970.8. ^{13}C NMR: γ_{C} (125.75 MHz, D_2O) ppm: 46.3 (CH_2); 76.3 (C-OH); 176.4 (CO_2H) $_{\beta}$; 179.8 (CO_2H) $_{\alpha}$; 192.9 (Rh- CO_2) $_{\beta}$; 195.3 (Rh- CO_2) $_{\alpha}$. UV-vis (H_2O , nm): 586 ($\pi^*(\text{RhRh}) \rightarrow \sigma^*(\text{RhRh})$); 442 ($\pi^*(\text{RhRh}) \rightarrow \sigma^*(\text{RhO})$); 292 ($\sigma(\text{RhO}) \rightarrow \sigma^*(\text{RhRh})$).

• Preparation of maghemite nanoparticles functionalized with Rhodium Compound, Magh-Rh₂(H₂cit)₄

Maghemite ($\gamma\text{-Fe}_2\text{O}_3$) nanoparticles were prepared according to procedures described previously [49]. Magnetite (Fe_3O_4) nanoparticles were synthesized by mixing FeCl_2 and FeCl_3 aqueous solutions (2:1 molar ratio) with NaOH solution under vigorous stirring. The solid was washed with distilled water until pH = 9 and oxidation of magnetite to maghemite was performed adjusting the pH to 3, stirring the dispersion under heating and constant oxygen flow. The reddish sediment was centrifuged, dispersed in water, and dialyzed for 24 hours.

In the second stage of the nanocomposite preparation procedure, the magnetic nanoparticles were functionalized with rhodium (II) citrate. For this purpose, 5 mL of the magnetic dispersion and 1 mL of rhodium (II) citrate solution (0.054 mol L^{-1}) were mixed and stirred for two hours at room temperature. The nanoparticles were separated by centrifugation (5000 rpm), washed three times with deionized water and thereafter dispersed in 5 mL of water. The stable magnetic solution containing Magh-Rh₂(H₂cit)₄ nanoparticles was obtained by adjusting the pH to 7.

• Preparation and characterization of Magnetoliposomes

A small unilamellar liposome based on L- α -phosphatidylcholine and L- α -lysophosphatidylcholine was made according to the modified injection method described elsewhere [28]. We used L- α -lysophosphatidylcholine because the formed vesicles are smaller and this leads to an increase in the permeability of the liposomal formulation through the cells [50]. Basically, 360 μL of an ethanolic solution containing 0.686 mM L- α -phosphatidylcholine, 0.0137 mM L- α -lysophosphatidylcholine, was injected with a syringe into 5 mL phosphate buffer solution (PBS), pH 7.4. The injection of 262 μL of maghemite nanoparticles with rhodium (II) citrate into PBS was performed at

56°C, under magnetic stirring at a flow rate 1 $\mu\text{L/s}$ to a final concentration of 1.96×10^{15} particle/mL.

Particle size and size distribution were obtained by laser light scattering using a particle size analyzer (Zetasizer, Malvern, UK). The magnetoliposome suspension containing the maghemite nanoparticles (Magh-Rh₂(H₂cit)₄) was analyzed in a 1.0 cm quartz cell. The measurement was performed in triplicates ($n = 3$). All experiments were carried out at 25°C in the range of 100-2000 Hz.

• Cell culture

MCF-7 human mammary carcinoma cell line (purchased from American Type Collection, ATCC, USA) and 4T1 murine mammary carcinoma cells (provided by Dr. Suzanne Ostrand-Rosenberg, Maryland, USA) were cultured in flasks (TPP, Switzerland) with Dulbecco's Modified Eagle's Medium (DMEM-Sigma, USA) containing 1% (v/v) penicillin-streptomycin (Sigma) and 10% (v/v) heat-inactivated fetal bovine serum (FBS-Gibco). Human normal breast cell line MCF-10A (donated by Dr. Maria Mitzi Brentani, USP, Brazil) was cultured with a 1:1 mixture of DMEM and F12 medium (Sigma) supplemented with 5% horse serum (Gibco), hydrocortisone (0.5 $\mu\text{g/mL}$, Sigma), insulin (1 mg/mL , Sigma), epidermal growth factor (20 ng/mL , Sigma), choleric toxin (100 ng/mL , Sigma) and 1% (v/v) penicillin-streptomycin. Cells were maintained at 37°C in humidified atmosphere with 5% CO_2 .

• Cell treatment

Cells were seeded into 6 or 96 well culture microplates at a density of 1.4×10^4 cells/ cm^2 and incubated for 24 h to allow cell's adhesion. Then cells were incubated with free Rh₂(H₂cit)₄ (50-600 μM), Magh-Rh₂(H₂cit)₄, and Lip-Magh-Rh₂(H₂cit)₄ (50 μM of Rh₂(H₂cit)₄) for 24, 48, and 72 h. As negative control, cells were incubated with maghemite nanoparticles and magnetoliposomes without Rh₂(H₂cit)₄ at the same equimolar iron concentrations found in Magh-Rh₂(H₂cit)₄ (23 mM, 3×10^{15} iron particles/mL) and Lip-Magh-Rh₂(H₂cit)₄ (94.5 mM, 12.5×10^{15} iron particles/mL), respectively. Untreated cells correspond to the control group, while cells treated with paclitaxel, a chemotherapy widely used in clinics, represent the positive control used to validate the model cells. An equimolar dose of Rh₂(H₂cit)₄ was used in the treatment of cells with paclitaxel (50 micromolar) to compare their cytotoxicity. Dimethyl sulfoxide (DMSO) was used as the paclitaxel treatment control.

• Cell viability assay

Cell viability was estimated by MTT (Invitrogen, USA) assay. After treatment, as described above, cells were incubated with 15 μL of MTT (5 mg/mL) and 185 μL of

culture medium for two and half hours at 37°C in humidified atmosphere with 5% CO₂. Then the culture solution was removed and 200 µL of DMSO was added. The absorbance readings were performed by spectrophotometer (SpectraMax M2, Molecular Devices) using a microplate reader at a 595 nm wavelength. The relative cell viability (%) was calculated by the formula: [A]treatment/[A]control × 100, where [A]treatment is the absorbance of the tested sample and [A]control is the absorbance of control sample (containing only culture medium).

• Cell morphology and ultra-structural analysis

The morphology and ultra-structural analysis were carried out after 48 h of treatment with free Rh₂(H₂cit)₄ (50 and 500 µM). Cell morphology was visualized by AxioSkop light microscope (Zeiss, Germany) and images were captured using AxioVision (Zeiss) software. For ultra-structural analysis, cells were washed with PBS and fixed for 1 h in solution containing 2% glutaraldehyde (v/v), 2% (w/v) paraformaldehyde, and 3% (w/v) sucrose in 0.1 M sodium cacodylate buffer pH 7.2. Afterward, cells were rinsed in the same buffer and post fixed, for 40 minutes, in 1% osmium tetroxide (w/v) and 0.8% potassium ferricyanide (10 mM CaCl₂ in 0.2 M sodium cacodylate buffer). The material was washed in distilled water and the block stained was performed for 12 h with 0.5% uranyl acetate at 4°C. Then samples were dehydrated in a graded acetone series (50-100%) for 10 minutes each and embedded in Spurr resin. Ultrathin sections were observed in a Jeol[®] 1011 transmission electron microscope (MET) at 80 kV.

• Annexin-V/propidium iodide staining analysis

After treatments with 50 and 500 µM of free Rh₂(H₂cit)₄, cells (1 × 10⁶ cels/mL) were washed with PBS and resuspended in the solution containing 100 µL of binding buffer (10 mM of HEPES/NaOH (pH 7.4), 140 mM NaCl, 2.5 mM CaCl₂), 5 µL of annexin-V-FITC (Biosource, USA) and propidium iodide (5 µg/mL, Invitrogen). In this step, cells were incubated for 15 minutes in the dark at room temperature. Next, 400 µL of binding buffer were added to the cells and 10,000 events for each sample were acquired by flow cytometry (Becton & Dickenson, San Jose, CA-USA). After acquisition, the analysis was done by software Cell Quest[™]. Cells without staining with annexin and propidium iodide (PI) were used as negative control of fluorescence.

• Actin filaments and nucleus staining analysis

Firstly, poly-L-lysine (1%) was added to coverslips placed in six well culture microplates and incubated overnight at 4°C. Cells were then attached to coverslips and, after 48 h of treatments with free Rh₂(H₂cit)₄ (50 and 500 µM), they were washed with PBS and fixed with 3.5%

paraformaldehyde for ten minutes at room temperature (RT). Next, the cells were permeabilized with 0.1% Triton-PBS for three minutes, washed with PBS, and incubated with 1% bovine serum albumin (BSA) for 30 minutes. Subsequently, the cells were stained with solution containing 2.5% Phalloidin-Alexa-Fluor 488 and 1% BSA (v/v) for 20 minutes and, after this time, 1 µg/mL of DAPI (4',6-diamidino-2-fenilindol) was added to cells for seven minutes in the dark at RT. The cells were washed twice with water, five minutes each, and then the coverslips were placed in slides with 4% N-propyl galate. Afterwards, the cells were examined and images were captured by laser scanning confocal microscopy (Leica SP5). All microscopy gain and offset settings were maintained constant throughout the study.

• Statistical Analysis

To determine the difference in the cell line's viability and in the annexin-V/propidium iodide staining among treatment groups over treatment time and cell line, an analysis of variance (ANOVA) with general linear model procedure followed by post hoc Tukey or Dunnett's test was used. Data were presented as mean value ± SEM of at least two independent experiments (SPSS, Inc., Chicago, IL, version 17.0). The IC₅₀ or EC₅₀ values and their 95% confidence intervals (CI 95%) were obtained by nonlinear regression (Sigma Stat; Prism 5.0; GraphPad Software Inc., San Diego, CA). The significance level was set at p < 0.05. In order to characterize the nanoparticles' size and morphology, the experimental data were fitted to a curve using a log-normal distribution function, and the modal diameter was obtained (SPSS, Inc., Chicago, IL, version 17.0).

Acknowledgements

This research was supported by the "Conselho Nacional de Desenvolvimento Científico e Tecnológico" (CNPQ), "Coordenação de Aperfeiçoamento de Pessoal de Nível Superior" (CAPES), "Fundação de Apoio a Pesquisa no Distrito Federal" (FAP-DF, Grant: 193.000.466/08) and "Financiadora de Estudos e Projetos" (FINEP). The authors are grateful to Prof. Ricardo Bentes de Azevedo for his laboratory support and to Prof. Antônio Raimundo Lima Cruz Teixeira for supplying the flow cytometry equipment. We also thank Ms. Graziella Anselmo Joanitti for her important technical support on flow cytometry proceedings and Calliandra Maria de Souza Silva for her English revision.

Author details

¹Instituto de Ciências Biológicas, Universidade de Brasília (UnB), Brazil. 70.919-970. ²Instituto de Química, Universidade Federal de Goiás (UFG), Brazil.74.001-970. ³Departamento de Química, Laboratório de Fotobiologia e Fotomedicina, Faculdade de Filosofia, Ciências e Letras de Ribeirão Preto, Universidade de São Paulo, 14040-901, Ribeirão Preto-SP, Brazil.

Authors' contributions

MLBC was the principal investigator and takes primary responsibility for the paper. MLBC, ZGML, ARS* and SNB participated in the design of the study and SNB co-ordinated the research; MLBC, ESN, RCAP, RGSO and LHML performed the laboratory work for this study; ESN and ARS* synthesized the rhodium (II) citrate and rhodium (II) citrate-loaded nanoparticles; ARS# and

ACT encapsulated the rhodium (II) citrate-loaded nanoparticles in liposomes, ICRS was responsible for statistical analysis; MLBC, ESN, ARS* and ARS# wrote the manuscript and all authors read and approved the final manuscript.

* Aparecido R de Souza

Andrea R Simioni

Competing interests

We also report that the University of Brasilia has submitted a patent application (in the Brazilian Patent Office - intellectual property number: 01211000013) to license the technology involved. The authors disclose no other potential conflicts of interest.

Received: 16 December 2010 Accepted: 28 March 2011

Published: 28 March 2011

References

1. Coughlin SS, Ekwueme DU: **Breast cancer as a global health concern.** *Cancer Epidemiol* 2009, **33**:315-318.
2. Kostova I: **Platinum complexes as anticancer agents.** *Recent Pat Anticancer Drug Discov* 2006, **1**:1-22.
3. Zhang CX, Lippard SJ: **New metal complexes as potential therapeutics.** *Curr Opin Chem Biol* 2003, **7**:481-489.
4. Katsaros N, Anagnostopoulou A: **Rhodium and its compounds as potential agents in cancer treatment.** *Crit Rev Oncol Hematol* 2002, **42**:297-308.
5. Junicke H, Hart JR, Kisko J, Glebov O, Kirsch IR, Barton JK: **A rhodium (III) complex for high-affinity DNA base-pair mismatch recognition.** *Proc Natl Acad Sci USA* 2003, **100**:3737-3742.
6. Angeles-Boza AM, Chifotides HT, Aguirre JD, Chouai A, Fu PK, Dunbar KR, Turro C: **Dirhodium(II, II) complexes: molecular characteristics that affect in vitro activity.** *J Med Chem* 2006, **49**:6841-6847.
7. Zyngier S, Kimura E, Najjar R: **Antitumor effects of rhodium (II) citrate in mice bearing Ehrlich tumors.** *Braz J Med Biol Res* 1989, **22**:397-401.
8. Gupta AK, Gupta M: **Synthesis and surface engineering of iron oxide nanoparticles for biomedical applications.** *Biomaterials* 2005, **26**:3995-4021.
9. Namdeo M, Saxena S, Tankhiwale R, Bajpai M, Mohan YM, Bajpai SK: **Magnetic nanoparticles for drug delivery applications.** *J Nanosci Nanotechnol* 2008, **8**:3247-3271.
10. Maeda H, Wu J, Sawa T, Matsumura Y, Hori K: **Tumor vascular permeability and the EPR effect in macromolecular therapeutics: a review.** *J Control Release* 2000, **65**:271-284.
11. Asadishad B, Vossoughi M, Alamzadeh I: **In vitro release behavior and cytotoxicity of doxorubicin-loaded gold nanoparticles in cancerous cells.** *Biotechnol Lett* 2010, **32**:649-654.
12. Kohler N, Sun C, Wang J, Zhang M: **Methotrexate-modified superparamagnetic nanoparticles and their intracellular uptake into human cancer cells.** *Langmuir* 2005, **21**:8858-8864.
13. Dreaden EC, Mwakwari SC, Sodji QH, Oyelere AK, El-Sayed MA: **Tamoxifen-poly(ethylene glycol)-thiol gold nanoparticle conjugates: enhanced potency and selective delivery for breast cancer treatment.** *Bioconjug Chem* 2009, **20**:2247-2253.
14. Ma G, Yang J, Zhang L, Song C: **Effective antitumor activity of paclitaxel-loaded poly (varepsilon-caprolactone)/pluronic F68 nanoparticles after intratumoral delivery into the murine breast cancer model.** *Anticancer Drugs* 2011, **21**:261-269.
15. Kettering M, Zom H, Bremer-Streck S, Oehring H, Zeisberger M, Bergemann C, Hergt R, Halbhuber KJ, Kaiser WA, Hilger I: **Characterization of iron oxide nanoparticles adsorbed with cisplatin for biomedical applications.** *Phys Med Biol* 2009, **54**:5109-5121.
16. Douziech-Eyrolles L, Marchais H, Herve K, Munnier E, Souce M, Linossier C, Dubois P, Chourpa I: **Nanovectors for anticancer agents based on superparamagnetic iron oxide nanoparticles.** *Int J Nanomedicine* 2007, **2**:541-550.
17. Sun YK, Ma M, Zhang Y, Gu N: **Synthesis of nanometer-size maghemite particles from magnetite.** *Colloids and Surfaces A: Physicochemical and Engineering Aspects* 2004, **245**:15-19.
18. **International Center of Diffraction Data.** *PDF Card 22-1086* 2000.
19. Batlle X, Labarta A: **Finite-size effects in fine particles: magnetic and transport properties.** *Journal of Physics D: Applied Physics* 2002, **35**:15-42.
20. Lu AH, Salabas EL, Schuth F: **Magnetic nanoparticles: synthesis, protection, functionalization, and application.** *Angewandte Chemie* 2007, **46**:1222-1244.
21. Bellamy LJ: **The Infrared Spectra of Complex Molecules.** Chapman and Hall; 3 1975.
22. Drmota A, Kosak A, Znidarsic A: **A mechanism for the adsorption of carboxylic acids onto the surface of magnetic nanoparticles.** *Materials and Technology* 2008, **42**:79-83.
23. Boyar EB, Robinson SD: **Rhodium(II) Carboxylates.** *Coordination Chemistry Reviews* 1983, **50**:109-208.
24. Deng YF, Jiang YQ, Hong QM, Zhou ZH: **Speciation of water-soluble titanium citrate: Synthesis, structural, spectroscopic properties and biological relevance.** *Polyhedron* 2007, **26**:1561-1569.
25. Zhou ZH, Hou SY, Cao ZX, Tsai KR, Chow YL: **Syntheses, spectroscopies and structures of molybdenum(VI) complexes with homocitrate.** *Inorganic Chemistry* 2006, **45**:8447-8451.
26. Najjar R, Santos FS, Seidel W: **Synthesis and characterization of the rhodium(II) citrate complex.** *Anais da Academia Brasileira de Ciências* 1987, **59**:1-2.
27. Liu ZL, Wang HB, Lu QH, Du GH, Peng L, Du YQ, Zhang SM, Yao KL: **Synthesis and characterization of ultrafine well-dispersed magnetic nanoparticles.** *Journal of Magnetism and Magnetic Materials* 2004, **283**:248-262.
28. Simioni AR, Pelisson MM, Beltrame M, Tedesco AC: **Photophysical and photobiological studies of a silicon tribenzonaphthoporphyrinato incorporated into liposomes for photodynamic therapy use.** *J Nanosci Nanotechnol* 2008, **8**:3208-3215.
29. de Souza AR, Najjar R, Glikmanas S, Zyngier SB: **Water-soluble rhodium(II) carboxylate adducts: cytotoxicity of the new compounds.** *J Inorg Biochem* 1996, **64**:1-5.
30. Howard RA, Kimball AP, Bear JL: **Mechanism of action of tetra-mu-carboxylatodirhodium(II) in L1210 tumor suspension culture.** *Cancer Res* 1979, **39**:2568-2573.
31. de Souza AR, Coelho EP, Zyngier SB: **Comparison of the anti-neoplastic effects of dirhodium(II) tetrapropionate and its adducts with nicotinate and isonicotinate anions in mice bearing Ehrlich tumors.** *Eur J Med Chem* 2006, **41**:1214-1216.
32. Chifotides HT, Dunbar KR: **Interactions of metal-metal-bonded antitumor active complexes with DNA fragments and DNA.** *Acc Chem Res* 2005, **38**:146-156.
33. Gottlieb E, Armour SM, Harris MH, Thompson CB: **Mitochondrial membrane potential regulates matrix configuration and cytochrome c release during apoptosis.** *Cell Death Differ* 2003, **10**:709-717.
34. Mizushima N: **Methods for monitoring autophagy.** *Int J Biochem Cell Biol* 2004, **36**:2491-2502.
35. Turcotte S, Giaccia AJ: **Targeting cancer cells through autophagy for anticancer therapy.** *Curr Opin Cell Biol* 2011, **22**:246-251.
36. Alberti C: **Cytoskeleton structure and dynamic behaviour: quick excursus from basic molecular mechanisms to some implications in cancer chemotherapy.** *Eur Rev Med Pharmacol Sci* 2009, **13**:13-21.
37. Rosenblum MD, Shivers RR: **'Rings' of F-actin form around the nucleus in cultured human MCF7 adenocarcinoma cells upon exposure to both taxol and taxotere.** *Comp Biochem Physiol C Toxicol Pharmacol* 2000, **125**:121-131.
38. Jordan MA, Wilson L: **Microtubules and actin filaments: dynamic targets for cancer chemotherapy.** *Curr Opin Cell Biol* 1998, **10**:123-130.
39. Kwok JC, Richardson DR: **The iron metabolism of neoplastic cells: alterations that facilitate proliferation?** *Crit Rev Oncol Hematol* 2002, **42**:65-78.
40. Petri-Fink A, Chastellain M, Juillerat-Jeanneret L, Ferrari A, Hofmann H: **Development of functionalized superparamagnetic iron oxide nanoparticles for interaction with human cancer cells.** *Biomaterials* 2005, **26**:2685-2694.
41. Sinisterra RD, Shastri VP, Najjar R, Langer R: **Encapsulation and release of rhodium(II) citrate and its association complex with hydroxypropyl-beta-cyclodextrin from biodegradable polymer microspheres.** *J Pharm Sci* 1999, **88**:574-576.
42. Burgos AE, Belchior JC, Sinisterra RD: **Controlled release of rhodium (II) carboxylates and their association complexes with cyclodextrins from hydroxyapatite matrix.** *Biomaterials* 2002, **23**:2519-2526.

43. Lacava ZGM, Azevedo RB, Martins EV, Lavava LM, Freitas MLL, Garcia VAP: **Biological effect of magnetic fluids: toxicity studies.** *Journal of magnetism and magnetic materials* 1999, **201**:431-434.
44. Morais PC, Santos RL, Pimenta ACM, B AR, D LEC: **Preparation and characterization of ultra-stable biocompatible magnetic fluids using citrate-coated cobalt ferrite nanoparticles.** *Thin solid films* 2006, **515**:266-270.
45. de Freitas ER, Soares PR, Santos Rde P, dos Santos RL, da Silva JR, Porfirio EP, Bao SN, Lima EC, Morais PC, Guillo LA: **In vitro biological activities of anionic gamma-Fe₂O₃ nanoparticles on human melanoma cells.** *J Nanosci Nanotechnol* 2008, **8**:2385-2391.
46. Sahu SK, Mallick SK, Santra S, Maiti TK, Ghosh SK, Pramanik P: **In vitro evaluation of folic acid modified carboxymethyl chitosan nanoparticles loaded with doxorubicin for targeted delivery.** *J Mater Sci Mater Med* 2010, **5**:1587-97.
47. Bear JL, Gray HB, Rainen L, Chang IM, Howard R, Serio G, Kimball AP: **Interaction of Rhodium(II) carboxylates with molecules of biologic importance.** *Cancer Chemother Rep* 1975, **59**:611-620.
48. Jeffery GH, Basset J, Mendham J, Denney RC: **VOGEL'S Textbook of quantitative chemical analysis.** New York: Longman Scientific & Technical; 5 1989.
49. Kang YS, Risbud S, Rabolt JF, Stroeve P: **Synthesis and characterizations of nanometer-size Fe₃O₄ and g-Fe₂O₃ particles.** *Chemistry of Materials* 1996, **8**:2209-2211.
50. Ralston E, Blumenthal R, Weinstein JN, Sharrow SO, Henkart P: **Lysophosphatidylcholine in liposomal membranes. Enhanced permeability but little effect on transfer of a water-soluble fluorescent marker into human lymphocytes.** *Biochimica et Biophysica Acta (BBA) - Biomembranes* 1980, **597**:543-551.

doi:10.1186/1477-3155-9-11

Cite this article as: Carneiro *et al.*: Free Rhodium (II) citrate and rhodium (II) citrate magnetic carriers as potential strategies for breast cancer therapy. *Journal of Nanobiotechnology* 2011 **9**:11.

**Submit your next manuscript to BioMed Central
and take full advantage of:**

- Convenient online submission
- Thorough peer review
- No space constraints or color figure charges
- Immediate publication on acceptance
- Inclusion in PubMed, CAS, Scopus and Google Scholar
- Research which is freely available for redistribution

Submit your manuscript at
www.biomedcentral.com/submit

